Synthesis and Crystal Structure of Maricite and Sodium Iron(III) Hydroxyphosphate

John. N. Bridson,* Sean E. Quinlan, and Peter R. Tremaine*

Department of Chemistry, Memorial University of Newfoundland, St. John's, Newfoundland, Canada A1B 3X7

Received July 8, 1997. Revised Manuscript Received December 10, 1997

Maricite and sodium iron hydroxyphosphate (SIHP) are recently discovered iron(II) and iron(III) compounds that play a major role in phosphate "hideout" and corrosion in high-pressure boilers. This paper reports a novel method for synthesizing maricite by thermally decomposing the complex of aqueous iron(III) nitrilotriacetic acid at 200 °C and methods for the hydrothermal synthesis of SIHP from Fe_3O_4 or $FePO_4$. The crystal structure of maricite is identical to the impure natural mineral (Le Page Y.; Donnay G. *Can. Mineral.* **1977**, *15*, 518−521). The X-ray diffraction pattern of SIHP is consistent with an orthorhombic unit cell containing 8 units of formula $Na_3Fe(PO_4)_2{\cdot}(Na_{2(1-x)}H_{2x}O)$, with $x = 0.226 \pm 0.025$. This is similar, but not identical, to the formula $Na_4Fe(OH)(PO_4)_2{\cdot}{}^1/_3NaOH$ proposed by Ziemniak and Opalka (*Proc. Sixth Int. Symp. on Environmental Degradation of Materials in Nuclear Power Systems—Water Reactors*; Gold, R. E., Simonen, E. P., Eds.; Mater., Metals, Minerals Soc., 1993; pp 929−935.). The main structural feature is a chain of iron(III) ions linked by bridging oxygens and phosphate bridges. The iron phosphate chains are held together by sodium ions in the ratio 3Na/Fe/2(PO_4). Charge balance with the O^{2-} bridge between each iron ion is maintained by Na^+ and H^+ ions located in a relatively open cage in the phosphate lattice. The structure is significant in that it explains the variable stoichiometry observed in powder diffraction patterns, and it identifies the stoichiometry of H and O, which cannot be determined from solubility studies.

Introduction

Most fossil-fired electrical power generating stations employ low concentrations of sodium phosphate to control boiler-water pH. Sodium phosphate "hideout" has been identified as a cause of major corrosion problems in some stations operating within the 1986 interim consensus guidelines.[1−3] Hideout in high-pressure boilers is characterized by the retention of phosphate in the boiler during operation at high temperatures and the subsequent release of phosphate into boiler water when the operating temperature is lowered. The effect is now known to be caused by reversible reactions between aqueous phosphate and magnetite that result in the formation of sodium iron phosphate compounds in local sites where the aqueous phosphate is concentrated by partial boiling or other means.[4−14] Experience in many stations suggests that appropriate phosphate water treatments can be safely used,[2,15] and several laboratories are now engaged in research to identify the mechanisms for the deleterious reactions.

(1) Ashoff, A. F.; Lee, Y. H.; Sopocy, D. M.; Jonas, O. Interim Consensus Guidelines on Fossil Plant Cycle Chemistry. *EPRI Report CS-4629*; (Electric Power Research Institute: Palo Alto, CA, 1986.

(2) Dooley, R. B. Cycle Guidelines for Fossil Plants: Phosphate Treatment for Drum Units. *EPRI Report TR-103665*; Electric Power Research Institute: Palo Alto, CA, 1994.

(3) Layton, K. F. Waterside Corrosion in the Water Wall Tubes of Hunter Unit 3. *Proc. EPRI Conf. Boiler Tube Failure in Fossil Plants (Atlanta, GA., 1987)*; Electric Power Research Institute: Palo Alto, CA, 1987.

(4) Economy, G.; Panson, A. J.; Liu, Chia-Tsun; Esposito, J. N.; Lindsay, W. T. Sodium Phosphate Solutions at Boiler Conditions: Solubility, Phase Equilbria and Interactions with Magnetite. *Proc. 36th Int. Water Conf.*; (Pittsburgh, October, 1975); pp 161−173.

(5) Connor, W. M.; Panson, A. J. Investigation of Phosphate-Sludge Interactions. *EPRI Report NP-2963*; Electric Power Research Institute: Palo Alto, Ca, 1983.

(6) Broadbent, D.; Lewis, G. G.; Wetton, E. A. M. The Chemistry of High Temperature Phosphate Solutions in Relation to Steam Generation. *Proc. BNES Conf. Water Chem. Nuclear Reactor Syst.*; London, 1978); pp 53−62.

(7) Broadbent, D.; Mackenzie, J. P.; Wetton, E. A. M. High-Temperature Phosphate Chemistry, Part IV Corrosion of Mild Steel in Sodium Phosphate Solutions at 250°, 300° and 350 °C. *CEGB Research Report NW/SSD/RR/67/78;* Central Electricity Generating Board: Leatherhead, U.K., 1978.

(8) Wetton, E. A. M. High-Temperature Phosphate Chemistry in Relation to the Phosphate Treatment of Boilers. *CEGB Report No. NW/SSD/RM/58/80*; Central Electricity Generating Board, Leatherhead, U.K., 1980.

(9) Wetton, E. A. M.; MacKenzie, J. P. High-Temperature Phosphate Chemistry, Part V Corrosion of Mild Steel, 1 Percent and 9 Percent Cr Steels in Sodium Phosphate Solutions at 300 °C. *CEGB Research Report* NW/SSD/RR/99/80; Central Electricity Generating Board: Leatherhead, U.K., 1980).

(10) Galonian, G. E.; Ziemniak, S. E.; Opalka, E. P. Possible Local Chemistry Conditions for Attack of Ni Cr Fe Alloy Steam Generator Tubes. *Proc. EPRI Contractors Meeting on Intergranular Corrosion*; Clearwater Beach, Florida, FL, 1982.

(11) Ziemniak, S. E.; Opalka, E. P. Magnetite Stability in Aqueous Sodium Phosphate Solution at Elevated Temperatures. *Knolls Atomic Power Lab Report KAPL-4735*, 1992; *Ibid. Proc. 6th Int. Symp. on Environmental Degradation of Materials in Nuclear Power Systems—Water Reactors*; Gold, R. E.; Simonen, E. P., Eds.; Materials Metals, Minerals Soc., 1993; pp 929−935.

(12) Tremaine, P. R.; Gray, L. G.; Wiwchar, B.; Stodola, J.; Taylor, P. Sodium Phosphate Chemistry Under High-Pressure Utility Drum Boiler Conditions. *Can. Electrical Assoc. R&D Rep. 913-G-730*, 1992.

(13) Tremaine, P. R.; Gray, L. G.; Wiwchar, B.; Stodola, J.; Taylor, P. Phosphate Interactions With Metal Oxides Under High-Pressure Boiler Hideout Conditions. *Proc. 54th Int. Water Conference*; (Pittsburgh, October, 1993−; Paper IWC-93-35.

S0897-4756(97)00484-5 CCC: $15.00
Published on Web 02/12/1998

The principal hideout reaction products are maricite ($NaFePO_4$), sodium iron hydroxyphosphate ("$Na_4Fe(OH)(PO_4)_2 \cdot {}^1/_3NaOH$"), and solid solutions of iron(II) in cubic Na_3PO_4, $Na_{3-2x}Fe_xPO_4$.[11−14] Maricite is a recently discovered natural mineral[16] which has been observed in high-temperature corrosion studies[6−9,12,13] and in some power station deposits.[2] Sodium iron hydroxy phosphate (SIHP) is an iron(III) phase observed by Connor and Panson,[5] Broadbent et al.,[7] Ziemniak and Opalka,[11] and Tremaine et al.[12−14] SIHP is unstable in the presence of water at temperatures below about 180 °C.[6] Ziemniak and Opalka[11] have recovered SIHP from reaction product mixtures, and determined its approximate stoichiometry to be $Na_4Fe(OH)(PO_4)_2 \cdot {}^1/_3NaOH$. Variations in the X-ray powder diffraction data suggest that SIHP is slightly nonstoichiometric.[12] Although some thermodynamic and spectroscopic data have been reported,[11] its structure is unknown.

This paper reports hydrothermal methods for the synthesis of maricite and SIHP and the crystal structures of both compounds. The problems associated with recovering equilibrium phosphate phases from hydrothermal systems are formidable. The iron(III) phase, SIHP, redissolves in the presence of liquid water below 180 °C, and hydrates are known to form with other reaction products. Removal of water by evaporation to dryness at high temperatures may precipitate nonequilibrium phases or cause pyrophosphate condensation reactions.[17,18] In addition, maricite is sensitive to oxidation.[12−14,17] The syntheses described below were carried out in a simple cell that facilitates the filtration and isolation of reaction products from aqueous media at elevated temperatures. SIHP was synthesized under hydrothermal conditions from solid iron reactants, while maricite was successfully prepared by a method based on the hydrothermal decomposition of aqueous iron(III) trinitriloacetate.

Experimental Section

Chemicals and Materials. The following ACS reagent-grade sodium phosphate compounds were used in the synthesis: $Na_3PO_4 \cdot 12H_2O$ (Fisher Scientific, 98.9%), Na_2HPO_4 (Aldrich, 99+%), $NaH_2PO_4 \cdot 2H_2O$ (BDH, 99.0−101.0%), NaOH (BDH, 99%), Fe_2O_3 (Aldrich, 99+%, BDH, ∼97%), Fe_3O_4 (Aldrich, 98%), hydrated $FePO_4$ (Johnson-Matthey, $FePO_4 \cdot xH_2O$, $x \approx 2$), and Fe powder (BDH). The approximate particle size of the iron oxides, as estimated from electron microscopy, was ∼ 0.2 and ∼0.8 μm respectively for the Aldrich and BDH hematite and ∼0.6 μm for magnetite. The stoichiometry of the waters of hydration in the reagent-grade materials was confirmed by measuring the weight loss on drying overnight at 150 °C. Otherwise, the solids were used without purification.

Iron nitrilotriacetate (FeNTA) for the maricite synthesis was prepared by boiling 20 g of ammonium ferric sulfate, $NH_4Fe(SO_4)_2 \cdot 12H_2O$ (BDH, ACS reagent grade), with 8 g of H_3NTA (nitrilotriacetic acid, Aldrich, 99%) in 400 mL of deionized water for 1 h according to the reaction

$$Fe^{3+}(aq) + H_3NTA(aq) \rightleftharpoons FeNTA(s) + 3H^+(aq) \quad (1)$$

The resulting yellow-green solid was suction filtered, washed with cold deionized water, and dried in air overnight. All solutions were prepared from Nanopure water (resistivity >18 MΩ cm).

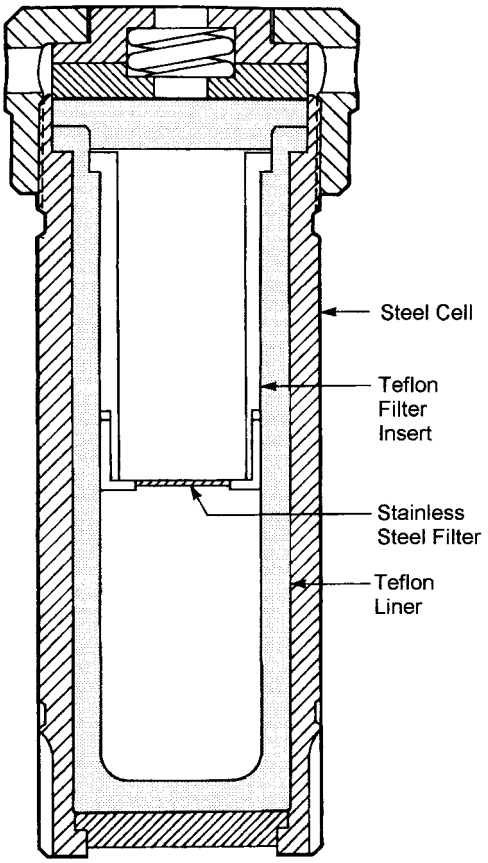

Figure 1. Modified Parr 4744 reaction vessels used for hydrothermal synthesis and in situ filtration.

Analytical Methods. Liquid samples taken from the reaction vessels were diluted by mass to approximately 50−250 ppm in sodium and phosphorus and analyzed using an ARL 3520 DES inductively coupled plasma emission spectrometer (ICP-ES). Solid products from the iron phosphate, hematite, magnetite, and iron nitrilotriacetate reactions were analyzed by scanning electron microscopy (SEM) at an accelerating voltage of 20 kV in a Hitachi S570 SEM equipped with a Tracor Northern 5500 energy-dispersive X-ray analyzer and a Microtrace Model 70152 silicon X-ray spectrometer. Powder X-ray diffraction (XRD) studies were done using a Rigaku RU-200 X-ray diffractometer with a 12 kW rotating anode Cu Kα X-ray source and a diffracted beam monochromator. Typically, the diffractometer was operated at 40 kV and 100 mA at a scan rate of 10° (2θ)/min. The JCPDS database with the software package MDI Jade+ was used for search-match studies where needed.

Synthesis and Characterization of Hideout Reaction Products. *Reaction Vessels and Methodology.* Modified Parr 4744 general purpose bombs were used to synthesize the solids at high temperature. These are 45 mL 316 stainless steel pressure vessels with Teflon liners. The liners were bored out to allow the insertion of an inner Teflon cup with a removable cap for holding a stainless steel filter, which divided the cell into upper and lower compartments. Filters were fabricated from 316 stainless steel mesh (100, 200, 325 mesh; Small Parts Inc., Miami Lakes, FL). A schematic diagram of this vessel is shown in Figure 1. This design allows in situ isolation of the

(14) Tremaine, P. R.; Quinlan, S.; Bridson, J.; Stodola, J. Solubility and Thermodynamics of Sodium Phosphate Reaction Products under Hideout Conditions in High-Pressure Boilers *Proc. 57th Int. Water Conference*; Pittsburgh, October, 1996; Paper IWC-96-21.

(15) Stodola, J. Ten Years of Equilibrium Phosphate Treatment. *Proc. 57th Int. Water Conference*; Pittsburgh, October, 1996; Paper IWC-96-20.

(16) LePage, Y.; Donnay, G. *Can. Mineral.* **1977**, *15*, 518−521.

(17) Taylor, P.; Tremaine, P. R.; Bailey, M. G. *Inorg. Chem.* **1979**, *11*, 2947−2953.

(18) Broadbent, D., Lewis, G. C.; Wetton, E. A. M. *J. Chem. Soc., Dalton Trans.* **1977**, *5*, 464−468.

solid reaction products from the aqueous phase by simply inverting the cell while in a high-temperature oven, to permit the liquid to drain through the stainless steel filter. Three small grooves on the outside of the inner liner avoided vapor-lock problems by allowing water vapor to escape from the bottom compartment while filtration took place.

Initially in all synthesis experiments, the solid starting materials were placed in the Teflon insert on top of the filter. The solution was placed in the Teflon cup, below the filter. Care was taken to ensure that the liquid level would be below the filter in both the upright and inverted positions, allowing for the thermal expansion of water. The vessel was then assembled and placed in a forced-air convection oven at 250 °C. By inverting the vessels, the solution was allowed to drain through the filter and react with the solid starting material. The vessels were maintained at 250 °C and shaken daily. After 1−4 weeks they were set upright in the oven for 1−5 h to filter the reaction product, then removed from the oven and placed on a cold aluminum plate. The resulting temperature gradient between the top and bottom of the vessels during cooling prevented condensation from forming on the reaction product and causing redissolution. Once the bombs were cooled to room temperature, they were opened under nitrogen, and the reaction products were transferred to a vacuum desiccator to avoid air oxidation.

Syntheses of Maricite. The hydrothermal synthesis of maricite requires reducing conditions or the use of reagents containing a low oxidation state of iron. Attempts to produce maricite from iron powder, according to the reaction

$$Na^+(aq) + Fe(s) + H_2PO_4^-(aq) \rightleftharpoons NaFePO_4(s) + H_2(g) \quad (2)$$

resulted in a poorly crystalline product that was very sensitive to air oxidation. Several unidentified reflections in the XRD powder pattern suggested the presence of other phases.

An alternative approach was suggested by the work of Booy and Swaddle,[19] who reported a procedure for the homogeneous precipitation of monodisperse crystallites of magnetite by thermally decomposing FeNTA(aq) in pressure vessels at 220 °C for 1 week. The synthesis of maricite was accomplished by carrying out the thermal decomposition in an aqueous sodium phosphate solution, according to the reaction

$$FeNTA(aq) + HPO_4^{2-}(aq) + Na^+(aq) \rightleftharpoons NaFePO_4(s) + \text{decomposition products of } HNTA^{2-}(aq) \quad (3)$$

using 0.6 g of FeNTA with 10 mL of 0.6 mol kg^{-1} aqueous $Na_{2.15}H_{0.85}PO_4$ solution in the vessel. At 250 °C the synthesis yields a product with needlelike crystals ~10 μm long, apparently arising from homogeneous nucleation followed by rapid growth from the nucleation site. A slight coloration was removed by washing with cold ethanol in a suction filter. This product is suitable for heat-of-solution, or other, dissolution experiments. At 200 °C the synthesis yielded platelike crystals, ~200 μm in diameter, suitable for single-crystal studies.

Syntheses of Sodium Iron Hydroxyphosphate (SIHP). SIHP was synthesized with iron(III) phosphate, hematite, and magnetite as the iron source, according to the following reactions:

$$3FePO_4(s) + 13Na^+(aq) + 3HPO_4^{2-}(aq) + 7OH^-(aq) \rightleftharpoons 3Na_4FeOH(PO_4)_2\cdot{}^1/_3NaOH(s) + 3H_2O(l) \quad (4)$$

$$3Fe_2O_3(s) + 26Na^+ + 12HPO_4^{2-}(aq) + 2OH^-(aq) \rightleftharpoons 6Na_4FeOH(PO_4)_2\cdot{}^1/_3NaOH(s) + 3H_2O(l) \quad (5)$$

$$2Fe_3O_4(s) + 26Na^+(aq) + 12HPO_4^{2-}(aq) \rightleftharpoons 6Na_4FeOH(PO_4)_2\cdot{}^1/_3NaOH(s) + 2H^+(aq) + H_2(aq) \quad (6)$$

Over 35 syntheses using reactions 4, 5, or 6 were carried out at 250 °C, with reaction times from 5 days to 4 weeks, and sodium−phosphate ratios in the range $2.15 \geq Na/P \geq 2.8$.

The optimum reaction conditions were achieved with Fe_3O_4 or $FePO_4$ as an iron source with the stoichiometric ratio of sodium and phosphate (Na/P = 2.15). An initial mass of 0.8−2.1 g of iron phosphate in the vessels, with initial concentrations of phosphate solution from 0.5 to 1.5 mol kg^{-1} yielded a product with no spurious powder XRD reflections. Syntheses from the iron oxides typically used 0.05−2.1 g of oxide, with initial concentrations of phosphate solution from 0.5 to 1.5 mol kg^{-1}. A reaction time of at least 3 weeks, with frequent agitation, was required to drive the reaction to completion. Under these conditions, the reaction proceeded to >99% completion as determined by powder XRD and elemental analysis, and the product was a red solid. Under the same conditions, the reaction with Fe_2O_3 proceeded to only 95% of completion.

When the vessels were removed before 3 weeks or if there was not sufficient agitation, the solids were usually yellow-green or red-yellow mixtures. Powder patterns of the yellow-green mixtures did not match previously reported patterns for SIHP, but the red-yellow mixtures did match. These results suggest that the reaction had not gone to completion and that the yellow-green solid was unreacted iron(III) phosphate.

Long single crystals (~200 μm long), suitable for XRD structural determinations, were obtained from corrosion experiments on carbon steel coupons, preoxidized to form a surface layer of Fe_3O_4, carried out at 250 °C in 0.84 mol kg^{-1} solutions of trisodium phosphate. The crystal used here for single-crystal XRD (dimensions 0.10 × 0.05 × 0.40 mm) was formed fortuitously during the preconditioning of a new stainless steel (Type 347) autoclave. A concentrated alkaline sodium phosphate solution (Na/P = 2.4; 0.84 mol kg^{-1} in phosphorus) containing a lesser amount of an inorganic oxidizing agent was heated beyond the expected threshold of reaction with magnetite. Upon opening the autoclave after continuous operation at 288 °C in a refreshed mode for 400 h, profuse growths of these reddish colored crystals were observed on the walls of the vessel.

Single-Crystal X-ray Diffraction. *Data Collection.* All measurements were made on a Rigaku AFC6S diffractometer with graphite-monochromated Mo Kα radiation and a 2KW sealed tube generator. The experimental parameters described below are for SIHP, in the first instance. The parameters for maricite are given in square brackets.

Cell constants and an orientation matrix for data collection were obtained from a least-squares refinement using the setting angles of 19 [14] carefully centered reflections in the range $44.29 < 2\theta < 49.21°$ [$47.54 < 2\theta < 49.50°$].

The data were collected at a temperature of 26 ± 1 °C using the $\omega-2\theta$ scan technique to a maximum 2θ value of 50.1°. ω scans of several intense reflections, made prior to data collection, had an average width at half-height of 0.33° [0.39°] with a takeoff angle of 6.0°. Scans of $(1.31 + 0.35 \tan\theta)°$ [$(1.84 + 0.35 \tan\theta)°$] were made at a speed of 4.0°/min (in ω). The weak reflections ($I < 10.0\,\alpha\,(I)$) were rescanned (maximum of two rescans), and the counts were accumulated to ensure good counting statistics. Stationary background counts were recorded on each side of the reflection. The ratio of peak counting time to background counting time was 2:1. The diameter of the incident beam collimator was 1.0 mm and the crystal to detector distance was 400.0 mm.

Data Reduction. A total of 848 [358] reflections was collected. The intensities of three representative reflections which were measured after every 150 reflections remained constant throughout data collection, indicating crystal and electronic stability (no decay correction was applied).

The linear absorption coefficient for Mo Kα X-rays for these crystals is 25.1 [53.2] cm^{-1}. An empirical absorption correction, based on azimuthal scans of several reflections, was

(19) Booy, M.; Swaddle, T. W. *Can. J. Chem.* **1978**, *56*, 402−403.

applied that resulted in transmission factors ranging from 0.87 to 1.00 [0.53 to 1.00]. The data were corrected for Lorentz and polarization effects. A correction for secondary extinction was applied (coefficient = 0.30529×10^{-6} [0.30964×10^{-5}]).

Structure Solution and Refinement. The structure was solved by direct methods.[20,21] The non-hydrogen atoms were refined anisotropically. The final cycle of full-matrix least-squares refinement[22] was based on 593 [272] observed reflections ($I > 2.00\sigma(I)$) and 97 [41] variable parameters and converged (the largest parameter shift was less than 0.005 times its estimated standard deviation) with unweighted and weighted agreement factors of

$$R = \sum||F_o| - |F_c||/\sum|F_o| = 0.034\ [0.026] \quad (7)$$

$$R_w = [(\sum w(|F_o| - |F_c|)^2/\sum wF_o^2)]^{1/2} = 0.036\ [0.031] \quad (8)$$

The standard deviation of an observation of unit weight[22] was 2.48 [2.69]. The weighting scheme was based on counting statistics and included a factor ($p = 0.01$) to downweight the intense reflections. Plots of $\sum w(|F_o| - |F_c|)^2$ versus $|F_o|$, reflection order in data collection, sin θ/λ, and maximum and minimum peaks on the final difference Fourier map corresponded to 0.45 and -0.74 e$^-$/Å^3 [0.61 and -0.51 e$^-$/Å^3], respectively.

Neutral atom scattering factors were taken from Cromer and Waber.[23] Anomalous dispersion effects were included in F_{calc};[24] the values of $\Delta f'$ and $\Delta f''$ were those of Cromer.[25] All calculations were performed using the TEXSAN[26] crystallographic software.

Crystal Structures. *Maricite.* The crystal structure and interatomic spacings obtained for maricite were very similar to those reported by LePage and Dornay[16] for a natural crystal with 10% of the Fe(II) sites substituted with Mn, Mg, and Ca. The crystal structure parameters are tabulated in Tables1 and 2. Details are given in the Supporting Information.

Sodium Iron(III) Hydroxyphosphate. The coordinates of the atoms are given in Tables 1 and 3, and the structure is shown in Figure 2.[27] The details of the analysis can be found in the Supporting Information. The X-ray diffraction pattern is consistent with an orthorhombic unit cell containing 8 units of formula $Na_3Fe(PO_4)_2\cdot(Na_{2(1-x)}H_{2x}O)$, with $x = 0.226 \pm 0.006$ where the uncertainty in x is the estimated standard deviation from the least-squares refinement. The theoretical XRD powder pattern for SIHP, calculated from the crystal structure, is presented in Table 4 along with the experimental powder pattern reported by Ziemniak and Opalka.[16] Ziemniak and Opalka indexed their powder pattern to a larger unit cell ($a' = 2a$) and, in view of this result, a search for reflections with half integral h indexes was undertaken. No such reflections were found, and we conclude that no superlattice with $a' = 2a$ was present in our crystal.

Table 1. Crystallographic Information

	SIHP	maricite
empirical formula	$Na_3Fe(PO_4)_2\cdot Na_{1.55}H_{0.45}O$	$NaFePO_4$
formula weight	366.85	173.81
crystal color	red, irregular	colorless, plate
crystal system	orthorhombic	orthorhombic
space group	*Ibam* (No. 72)	*Pnma* (No. 62)
Z value	8	4
lattice parameters	$a = 14.698$ Å	$a = 8.990$ Å
	$b = 15.522$ Å	$b = 6.862$ Å
	$c = 7.114$ Å	$c = 5.047$ Å
	$V = 1623$ Å	$V = 311.3$ Å
D_{calc}	3.002 g cm^{-3}	3.708 g cm^{-3}
F_{000}	1428	336
μ (Mo Kα)	25.11 cm^{-1}	53.17 cm^{-1}
temperature	26 °C	26 °C
$2\theta_{max}$	50.1°	50.0 °
corrections	Lorentz-polarization absorption trans. factors: 0.87−1.00 secondary extinction coefficient: 0.30529e-06	Lorentz-polarization absorption trans. factors: 0.53−1.00 secondary extinction coefficient: 0.30964e-05

Table 2. Positional Parameters for Maricite, $NaFePO_4$

atom	x	y	z	occupancy
Fe(1)	1/2	1/2	1/2	1/2
P(1)	0.3242(1)	1/4	0.0357(2)	1/2
Na(1)	0.6504(2)	1/4	−0.0296(4)	1/2
O(1)	0.3786(3)	0.4317(3)	0.1819(5)	1
O(2)	0.3838(4)	1/4	1/2	1/2
O(3)	0.1516(4)	1/4	1/2	1/2

Table 3. Positional Parameters for SIHP, $Na_3Fe(PO_4)_2\cdot Na_{1.55}H_{0.45}O$

atom	x	y	z	occupancy
Fe(1)	1/4	1/4	1/4	1/2
P(1)	0.3811(1)	0.3780(1)	1/2	1/2
P(2)	0.1209(1)	0.3833(1)	0	1/2
Na(1)	0.2701(2)	1/2	1/4	1/2
Na(2)	1/2	0.4721(3)	3/4	1/4
Na(3)	0	0.2628(2)	1/4	1/2
Na(4)	0.01384(2)	0.3814(2)	1/2	1/2
Na(5)	0	1/2	1/4	1/4
Na(6)	0.3806(4)	0.3777(1)	0	0.274
O(1)	0.3260(2)	0.3546(2)	0.3223(5)	1
O(2)	0.4732(3)	0.3347(3)	1/2	1/2
O(3)	0.3914(3)	0.4767(3)	1/2	1/2
O(4)	0.1482(2)	0.3329(2)	0.1790(5)	1
O(5)	0.0168(3)	0.3914(3)	0	1/2
O(6)	0.1656(4)	0.4720(3)	0	1/2
O(7)	0.3064(3)	0.2551(3)	0	1/2
H(1)	0.3296(1)	0.3052(1)	0	0.226

The precision of the x value was tested by refining the structure at the fixed values $x = 0.200$, 0.250, and 0.375. While the values in the range $0.20 \le x \le 0.25$ yielded only marginal differences in R, R_w, and the standard deviation, the value $x = 0.375$ yielded a significantly poorer fit ($R = 0.048$, $R_w = 0.057$, standard deviation = 3.94). We have therefore assigned an overall uncertainty of ±0.025 to the fitted value of $x = 0.226$.

Discussion

Synthetic Methods. The cell shown in Figure 1 provided a simple means to synthesize the equilibrium sodium iron phosphate phase of interest in an aqueous reaction medium, then to isolate and recover the solid while avoiding contact with liquid water. The temperature gradient between the top and bottom of the vessels during cooling provides an atmosphere of unsaturated water vapor in the upper chamber of the vessel which

(20) Gilmore, C. J. *J. Appl. Crystallogr.* **1984**, *17*, 42−46.
(21) Beurskens, P. T. DIRDIF: Direct Methods for Difference Structures—An Automatic Procedure for Phase Extension and Refinement of Difference Structure Factors. *Technical Report 1984/1 Crystallography Laboratory, Toernooiveld*, 6525 Ed Nijmegen, Netherlands.
(22) Least squares function minimized: $\sum w(|F_o| - |F_c|)^2$ where $w = 4F_o2/\sigma^2(F_o^2)$; $\sigma^2(F_o^2) = [S^2(C + R^2B) + (pF_o^2)^2]/Lp^2$; S = scan rate; C = total integrated peak count; R = ratio of scan time to background counting time; B = total background count; Lp = Lorentz-polarization factor; $p = p$ factor; standard deviation of an observation of unit weight: $[\sum w(|F_o| - |F_c|)^2/(N_o - N_v)]^{1/2}$ where: N_o = number of observations; N_v = number of variables.
(23) Cromer, D. T.; Waber, J. T. International Tables for X-ray Crystallography,. Kynoch Press: Birmingham, England, 1974; Vol. IV, Table 2.2 A.
(24) Ibers, J. A.; Hamilton, W. C. *Acta Crystallogr.* **1964**, *17*, 781−782.
(25) Cromer, D. T. International Tables for X-ray Crystallography; Kynoch Press: Birmingham, England, 1974; Vol. IV, Table 2.3.1.
(26) TEXSAN—Texray Structure Analysis Package, Molecular Structure Corp., 1985.
(27) Motherwell, S.; Clegg, W. PLUTO Program for Plotting Molecular and Crystal Structures, University of Cambridge, England, 1978.

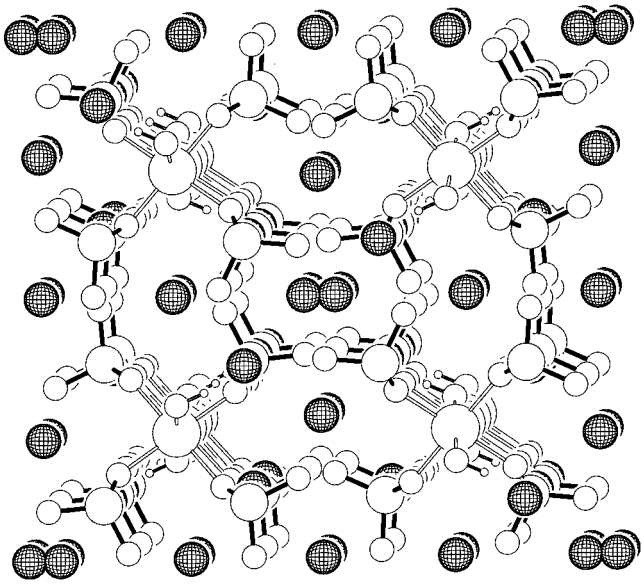

Figure 2. Unit cell of sodium iron(III) hydroxyphosphate, viewed along the *c* axis. Sodium ions are represented by crosshatched spheres. Other atoms are identified in the caption to Figure 3.

inhibits dehydration of the reaction products while avoiding condensation.

The synthesis of maricite in the vessel by the homogeneous decomposition of iron(III) NTA in aqueous sodium phosphate is a novel approach that may be suitable for the hydrothermal synthesis of other soluble iron(II) salts or minerals. Booy and Swaddle[19] have shown that the decomposition of the NTA^{3-}(aq) creates reducing conditions favorable for the homogeneous nucleation of magnetite. The formation of maricite, when the reaction was carried out in the presence of aqueous sodium phosphate, suggests that it may be the thermodynamically stable phase under these conditions. It seems probable that the method can be used as a general route for synthesizing crystalline and possibly monodisperse metal oxides or salts in low oxidation states by decomposing the NTA complex within the stability field of the desired product.

The synthesis of SIHP from solid reactants required longer reaction times and provided less control on the crystallinity of the product. Although it should be possibile to prepare SIHP by hydrothermal decomposition of iron(III) NTA or another complex, we were unable to identify a suitably oxidizing aqueous medium or alternative chelant in the course of this study.

Structure of Maricite. The crystal structure and atomic parameters for maricite listed in Tables 1 and 2 agree with those reported by Le Page and Donnay[16] for a mineral sample with the formula $Na(Fe_{0.90}Mn_{0.06}Mg_{0.03}Ca_{0.01})PO_4$ to within the combined experimental uncertainty. A full description is given in ref 16. Briefly, maricite is an ionic crystal, whose structure is of the high-temperature $CoSO_4$ type. The Na^+ ion is surrounded by 10 oxygen atoms within 10 Å in irregular coordination. The distorted octahedron around the iron is of the (2+2+2) type, and the phosphate tetrahedron is nearly regular. Half the oxygen atoms are coordinated to two Na, two Fe, and one P atoms, and the other half to three Na, one Fe, and one P atoms.

Table 4. Powder X-ray Pattern for SIHP, $Na_3Fe(PO_4)_2{\cdot}Na_{1.55}H_{0.45}O$

	calculated[a]		ref 11		ref 7[b]	
h k l	*d*/Å	intensity	*d*/Å	intensity	*d*/Å	intensity
0 2 0	7.7610	874	7.71	150	7.75	200
2 0 0	7.3490	919	7.31	350	7.34	200
2 2 0	5.3362	376	5.31	250	5.32	250
1 2 1	4.9392	31				
1 3 0	4.8804	46				
2 1 1	4.8550	899	4.84	100	4.85	450
0 4 0	3.8805	85				
4 0 0	3.6745	67				
2 3 1	3.6362	358	3.63	50	3.62	400
0 0 2	3.5570	10				
2 4 0	3.4315	73	3.42	50	3.42	100
4 2 0	3.3211	83	3.31	150	3.31	50
0 2 2	3.2336	297				
2 0 2	3.2017	294	3.21	50	3.21	300
2 2 2	2.9597	86			2.954	100
1 3 2	2.8745	29				
3 1 2	2.8301	25				
4 3 1	2.7610	10				
4 4 0	2.6681	1000	2.663	1000	2.656	800
2 5 1	2.6534	136				
3 5 0	2.6223	25				
0 4 2	2.6221	399	2.618	300	2.608	1000
0 6 0	2.5870	30				
5 3 0	2.5559	37				
4 0 2	2.5557	481	2.552	200	2.545	800
2 4 2	2.4696	12	2.513	50		
6 0 0	2.4497	100	2.443	50	2.459	50
1 6 1	2.3986	35				
1 5 2	2.3098	78			2.305	50
6 1 1	2.2908	20				
4 5 1	2.2497	26				
5 1 2	2.2422	95				
2 1 3	2.2333	137			2.236	100
5 4 1	2.2256	11				
1 7 0	2.1926	15				
4 4 2	2.1344	149	2.112	100	2.132	100
4 6 0	2.1153	125			2.108	50
7 1 0	2.0808	39				
6 4 0	2.0714	129	2.075	50	2.064	100
2 3 3	2.0686	16				
3 2 3	2.0580	23				
2 7 1	2.0343	27				
4 1 3	1.9762	198			1.971	100
7 3 0	1.9456	17				
0 8 0	1.9403	195	1.938	200	1.933	300
2 8 0	1.8760	34	1.872	50		

[a] Reflections with $I < 10$ are omitted. [b] Data from Broadbent et al.[6,7] cited by Ziemniak and Opalka,[11] and Tremaine et al.[12]

Structure of SIHP. The formula $Na_3Fe(PO_4)_2{\cdot}(Na_{2(1-x)}H_{2x}O)$, $x = 0.226$ is similar, but not identical, to the formula $Na_4Fe(OH)(PO_4)_2{\cdot}{}^1/_3NaOH$ proposed by Ziemniak and Opalka[11] from elemental analyses. The main structural feature, shown in Figures 2 and 3, is a chain of Fe(III) ions linked by bridging oxygens and phosphate bridges shown in Figure 4. The crystal structure analysis indicates that alternating iron and oxygen atoms with Fe−O−Fe and O−Fe−O angles of 129.8° and 180° respectively form zigzag chains parallel to the *c* axis. Iron lies at the center of symmetry and the Fe−Fe distances are 3.58 Å. Completing the metal coordination sphere are two phosphates linking adjacent irons. The phosphorus and ligating oxygen atoms lie on *m*. The structure can thus be visualized as a core of iron surrounded by an inner layer of coordinating oxygen atoms, one of which (O 7) bridges irons directly, the remainder belonging to phosphate ions. The outer layer of oxygen atoms carrying the balance of phosphate negative charge includes sodium

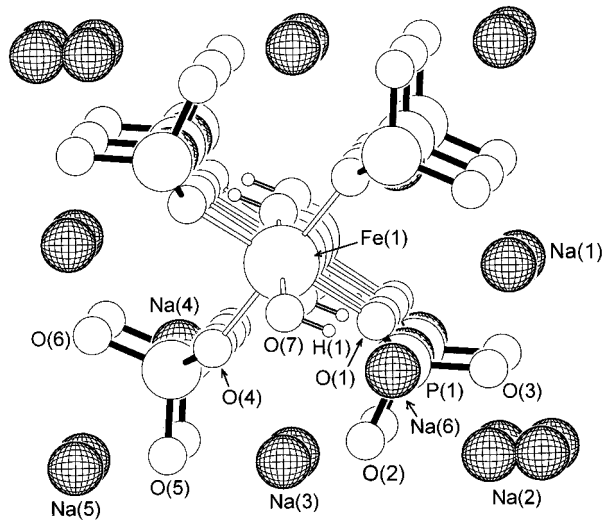

Figure 3. Details of the structure of sodium iron(III) hydroxyphosphate viewed along the iron(III) chain, showing the relative positions of the oxygen/hydroxide bridges, the coordinated phosphate ions, and sodium ions. Labels referring to atomic positions correspond to Table 2. The disordered sodium ion, Na(2), is shown by the dumbell-shaped atom. The proton H(1) and sodium Na(6) sites cannot be occupied simulaneously.

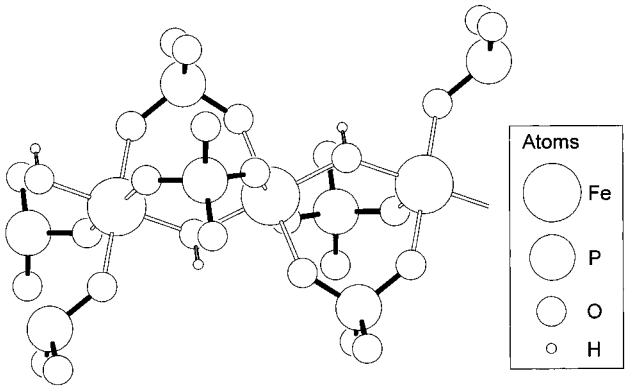

Figure 4. Structure of the iron(III) chain in sodium iron(III) hydroxyphosphate, showing the hydroxide and phosphate bridges, as viewed perpendicular to the *c* axis.

ions in five distinct sites. The analysis also indicates that the bridging oxygens of the central iron(III) core are associated with either a proton or a sixth sodium (Na 6) nonstoichiometrically and in a disordered fashion. The sodium ions close to *222* (Na 2) occupy one of two nearly identical sites, also in a disordered arrangement.

X-ray powder diffraction results of SIHP from different sources show slight variations in *d* spacings consistent with a nonstoichiometric structure.[12] Other structural information for SIHP is limited. Ziemniak and Opalka[11] have reported the Mössbauer and infrared spectra of SIHP. Results from their Mössbauer analysis showed that iron was distributed nearly equally between two distinct lattice sites, and that the iron ions in the crystal were entirely in the Fe(III) oxidation state. Absorption peaks at 3550 cm^{-1} (major) and 3580 cm^{-1} (minor) in the infrared spectrum[11] are consistent with the presence of hydroxyl ions.

The Mossbauer results confirm that the bridging $-OH$ and $-O^- Na^+$ groups along each chain are not ordered in an alternating pattern, which would leave every Fe(III) site equivalent. Nor can they be in a random arrangement, which would yield three possible permutations of Fe(III) sites [$-OH-Fe-OH-$, $-OH-Fe-O(Na)-$, and $-O(Na)\text{-}Fe-O(Na)-$] statistically distributed in an approximate ratio of 1:2:1. The presence of two iron sites of roughly equal abundance suggests the presence of long oligomeric chain segments, or separate chains, that are either all $-OH$ bridged or all $-O^-Na^+$ bridged. Ziemniak and Opalka reported a double unit cell ($a = 29.28$ Å, $b = 15.49$ Å, $c = 7.12$ Å) from powder X-ray diffraction data for a sample of SIHP with stoichiometry $x = 0.375$ (determined by elemental analysis), consistent with the presence of a superlattice resulting from regular alternation along the *a* axis of chains containing the two bridging groups. The fact that no strong superlattice was evident in our single crystal study suggests that a more realistic interpretation would have iron chains that include extended segments of oxide or hydroxide bridges distributed in a random fashion, with a bias toward regular alternation in samples that display the superlattice. It is reasonable to speculate that the completely disordered nonstoichiometric structure on one hand and a stoichiometric superlattice on the other are extremes in a range of structures dependent upon the exact conditions of crystallization. The disordered distribution of the (Na 2) sodium ions may be associated with the presence of the $-OH$ or $-O^-Na^+$ bridges. Although the hypothesis has not been tested, it is certainly possible that this sodium ion corresponds to two related but nonequivalent sites in the superlattice.

The structure is significant in that it explains the variable stoichiometry inferred from powder diffraction patterns in this and other work,[12] and it supports the possibility of a superlattice in the structure. The identification of the stoichiometry of hydrogen and oxygen, which cannot be determined from solubility studies or routine elemental analysis, is important for thermochemical studies now underway.

Acknowledgment. We are grateful to Dr. Steve Ziemniak, Mr. Jan Stodola, and Dr. Peter Taylor for helpful discussions, to Mr. David Miller for capable assistance with the XRD measurements, and to Mr. Randy Thorne for fabricating the pressure vessels. This research was supported by Ontario Hydro, the Canadian Electrical Association and the Natural Sciences and Engineering Research Council (NSERC) and by Memorial University of Newfoundland.

Supporting Information Available: Further details of the experimental conditions for the crystal structure of SIHP and maricite (12 pages); tables of structure factors (6 pages). Ordering information is given on any current masthead page.

CM9704847